Journal of Robotics and Control (JRC)
Volume 6, Issue 5, 2025
ISSN: 2715-5072, DOI: 10.18196/jrc.v6i5.26854

Boosting Energy for Building-Integrated Photovoltaic Cells using Novel Boost Converter with Voltage Multiplier Cell and ANN-MPPT

Mohammed Albaker Najm Abed [1*], Zahraa Shihab Al Hakeem [2], Maysoon Safi Yasir [3], Abduljabbar O. Hanfesh [4]
[1] Department of Computer Technology Engineering, Al Taff University College, Karbala, Iraq
[2] Department of Artificial Intelligent, College of The Engineering and Information Technology, Al-Zahraa University for Women, Karbala, Iraq
[3] Department of Architecture, College of The Engineering and Information Technology, Al-Zahraa University for Women, Karbala, Iraq
[4] Department of Electromechanical Engineering, University of Technology, Baghdad, Iraq
Email: [1] e09163265@s.uokerbala.edu.iq, [2] zahraa.shihab@alzahraa.edu.iq,[3] maysoon.safi@alzahraa.edu.iq,
[4] 50018@uotechnology.edu.iq
*Corresponding Author

***Abstract*—This study investigates optimizing photovoltaic (PV) energy delivery to building lighting loads by proposing a novel boost converter with a voltage multiplier stage (VMS) and an intelligent maximum power point tracking (MPPT) system. The research contribution is the design and comparative analysis of this advanced converter topology against a traditional boost converter to demonstrate enhanced performance under diverse operating conditions. The methodology involves simulating the PV system under four distinct scenarios including variations in load resistance, desired output voltage, and dynamic solar irradiance. The performance of three MPPT algorithms namely artificial neural network (ANN), particle swarm optimization (PSO), and perturb and observe (P&O), was evaluated to identify the most effective control strategy. The results by using MATLAB/Simulink show that the proposed boost VMS converter consistently outperforms the traditional boost converter by exhibiting improved power extraction and enhanced stability in output voltage and current. For example in a scenario with a 50 V output and 1000 W/m² irradiance the boost VMS converter achieved a more stable output power of approximately (961.52W) compared to (941.543W) from the traditional converter. Furthermore the ANN-based MPPT demonstrated superior stability and power tracking accuracy especially under dynamic irradiance conditions, where it maintained a stable output while PSO and P&O experienced significant power drops. Integrating the boost VMS converter with an ANN-based MPPT provides a superior, robust solution for optimizing PV energy utilization in building lighting applications, ensuring efficient and stable power delivery under fluctuating environmental and load conditions.**

Keywords—Photovoltaic (PV) Systems; Maximum Power Point Tracking (MPPT); Artificial Neural Network (ANN); Advance Boost Converter; Boost Voltage Multiplier Stage (VMS) Converter.

I. INTRODUCTION

Photovoltaic (PV) systems are becoming increasingly essential for sustainable energy generation with widespread applications in residential, commercial, and industrial sectors which including specialized fields like building-integrated photovoltaics (BIPV) [1], [2]. The applications of PV systems are widespread [3]-[6]. In residential settings, PV panels provide electricity for lighting, appliances, and electric vehicle charging [7]. Commercial buildings utilize PV systems to reduce energy costs and enhance sustainability. Industrial applications include powering manufacturing processes and electric machinery [8], [9]. BIPV systems integrate PV modules into the building envelope as a construction material and renewable energy source [10], [11].

A crucial aspect of maximizing the efficiency of these systems is the effective interfacing of the PV array with the load which is primarily achieved through DC/DC converters [12], [13]. These converters are play a critical role in adjusting the voltage and current levels to match the load requirements and optimizing power transfer [14].

While conventional DC/DC converters like the boost, buck, and buck-boost are widely used they often face limitations in achieving the high voltage gain and efficiency required for specific applications such as BIPV systems powering building lighting loads [15]-[18]. More advanced topologies like the converter with a voltage multiplier stage (VMS) explored in the research are designed to achieve higher voltage gain and improved efficiency [19].

Maximum power point tracking (MPPT) techniques are essential to further optimize the power extraction from PV panels and to control the DC/DC converter duty cycle to match the delivered power to the loads [20], [21]. The maximum power point (MPP) varies with the solar irradiance and temperature, necessitating MPPT algorithms to the continuously track and adjust the operating point of the PV array [22].

Traditional MPPT algorithms such as perturb and observe (P&O) and incremental conductance (INC), are common but can be slow to respond to rapid changes in solar irradiance or may fail to track the global maximum power point under partial shading conditions. In contrast an intelligent techniques like artificial neural networks (ANN), ANFIS, and particle swarm optimization (PSO) can learn the complex relationships between environmental conditions and the

maximum power point (MPP), offering more accurate and faster tracking [23]-[29]. However a significant gap exists in the integrated optimization of both converter topology and intelligent MPPT control for BIPV systems to ensure stable power delivery to lighting loads [30]-[33]. This research addresses this gap by proposing a novel boost converter with a voltage multiplier stage (VMS) to enhance voltage gain and efficiency, combined with an ANN-based MPPT to ensure accurate and reliable power tracking under dynamic operating scenarios. The contribution of this study is to compare the performance of this advanced converter and intelligent MPPT system with a traditional boost converter. The methodology involves simulating the system under various conditions, including different loads, voltage requirements, and solar irradiance levels, to comprehensively evaluate its effectiveness.

The rest of the paper is organized as follows: Section 2 details the methodology and mathematical models, including the BIPV system, converter topologies, and MPPT algorithms (ANN, PSO, and P&O). Section 3 presents the numerical results and analysis for each simulation scenario. Finally, Section 4 provides the conclusions and outlines potential future work.

II. METHODOLOGY

A. Photovoltaic Panel

Building-integrated photovoltaics (BIPV) are being considered or utilized in building design. BIPV refers to integrating photovoltaic materials into the building envelope, replacing traditional building materials in parts of the building such as the roof, facade, skylights, or windows. It contrasts with simply mounting PV modules on an existing building structure [34], [35].

BIPV systems offer several advantages. It generate electricity directly at the point of consumption that reducing transmission losses. BIPV can also offset the cost of traditional building materials as the PV modules serve a dual purpose: generating electricity and providing building envelope functions like weather protection and thermal insulation. Furthermore BIPV contributes to the aesthetic appeal of buildings, offering design flexibility and the potential for visually appealing integration of renewable energy technology. The research's photovoltaic (BIPV) system utilizes solar panels configured in an array to convert solar irradiance into electrical energy. The BIPV panel feeds the building load through a DC/DC converter or battery. The specific BIPV array is composed of four parallel strings, with each string containing two series-connected modules [36].

Table I provides the details of the BIPV panel used in the study. Below: The BIPV field comprises parallel and series modules to achieve the required power [37].

Fig. 1 shows a BIPV panel with two diode circuits. The two-diode BIPV model was selected over a single-diode model for its enhanced accuracy in representing the real-world behavior of a PV cell. While the single-diode model simplifies the cell's electrical characteristics it often fails to accurately account for the effects of recombination losses within the depletion region especially at low irradiance levels [38]-[40]. The dual-diode model by adding a second diode, directly incorporates these recombination effects. It makes it more precise in predicting the PV cell performance under various operating conditions that including the low light and dynamic shading scenarios often encountered in BIPV systems. The second diode also provides a better fit for the experimental data that leading to a more realistic and reliable simulation of the overall system. The BIPV panel I_V and P_V curves with different irradiance specifications are shown in Fig. 2. The maximum power from BIPV panels is 965.6 W at 1000 irradiance and 191.203 W at 400 irradiance. For the research on the mathematical modeling of a BIPV panel within the MATLAB-Simulink environment, the single-diode model offers a compelling balance between simplicity and accuracy, making it an ideal choice.

TABLE I. SPECIFICATIONS OF BIPV PANELS

Specification	Value	Unit
Module	Waaree Energies WU-120	
Maximum Power	120.7	W
Module-specific cells (Ncell)	72	
Voltage in the open circuit (Voc)	21	V
Current Short-circuit (Isc)	8	A
Maximum power point voltage (Vmp)	17	V

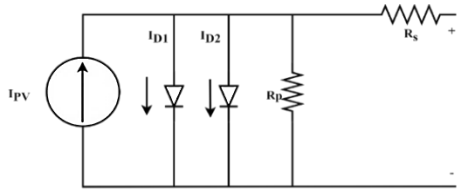

Fig. 1. Equivalent circuit of BIPV panel [41]

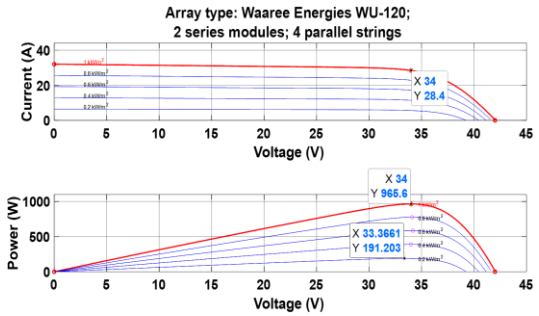

Fig. 2. BIPV panel I_V and P_V curve specification

The model was created using the following (1) [42]:

$$I_{ph} = [I_{sc} + K_i(T_c - T_{ref})]\frac{G}{G_{ref}} \quad (1)$$

The current at the junction is expressed as follows in (2):

$$I_d = I_{PV} - I_{01}[exp\left(\frac{V+IR_s}{a1V_{T_1}}\right) - 1] - I_{02}[exp\left(\frac{V+IR_s}{a2V_{T_2}}\right) - 1] - (\frac{V+IR_s}{R_p}) \quad (2)$$

The following (3) gives the current flowing through the resistance R_{sh}:

$$I_{sh} = \frac{(V+R_sI)}{R_{sh}} \quad (3)$$

whence

$$I = \left[I_{sc} + K_I\left(T_c - T_{ref}\right)\right]\frac{G}{G_{ref}} - I\left[\exp\left(\frac{q(V+R_sI)}{N.K.T}\right) - 1\right] - \frac{(V+R_sI)}{R_{sh}} \quad (4)$$

Where, I_d is the current across the diode (A), I_{01} and I_{02} are the diodes 1 and 2's reverse saturation currents, VT1 and VT2 are the corresponding diodes' thermal voltages, and a1 and a2 stand for the ideal constants of the diode. Several investigators believed that a_1 = 1 and a_2= 2. I_{sc} is the current of the short circuit (A), I_o is the current for diode saturation (A), I_1, I_2 is the BIPV panel's current is reverse saturation current (A) of the diode, V_{BIPV}: voltage across the diode, R_s is the series resistance (Ω) of the diode, R_{sh} is the shunt resistance of the diode (Ω), and V_{BIPV} is the diode voltage (V).

B. Advance DC/DC Converter

1. Boost Converter

Solar power systems and regulated DC power supplies are the only two examples of the many power electronic applications for the traditional boost converter. The beneficial is to increase the DC output voltage of the desired load from a low DC input voltage [43], [44]. There are two current operating modes for the converter. There are two types of current modes: continuous (CCM) and discontinuous (DCM). The traditional boost converter can function at many power levels and in any current mode in power applications, and every setting has unique variation features [45]. Table II details the boost converter used in the study [46].

TABLE II. THE BOOST CONVERTER PARAMETERS

Parameter	Value
Input capacitance C_{boost}	781.25×10^{-6} F
Inductance	12.14×10^{-6} H

When the switch is closed, the diode is reverse-biased. Around the path, including the closed switch, inductor, and source indicated in (5) the Kirchhoff's voltage law is applied [47].

$$v_L = V_{PV} = L\frac{di_t}{dt} \quad (5)$$

Here is (δ) the duty cycle, (v_L) is the inductors voltage across it, (V_{PV}) is the BIPV panels terminal voltage, and (L) is the boost converter inductor.

The diode becomes forward-biased when the switch is opened that creating a channel for the inductor current. It prevents the inductor current from changing instantly. When the output voltage V_o is in (6) the voltage across the inductor remains constant.

$$v_L = V_{PV} - V_o = L\frac{di_L}{dt} \quad (6)$$

From (7), the calculation of the output voltage (V_o),

$$V_o = \frac{V_{PV}}{1-\delta} \quad (7)$$

The average values of (8) and (9) and the variation in current are used to calculate the maximum and minimum inductor currents.

$$I_{max} = I_L + \frac{\Delta i_L}{2} = \frac{V_{PV}}{(1-\delta)^2 R_{load}} + \frac{V_{PV}\delta T}{2L} \quad (8)$$

$$I_{min} = I_L - \frac{\Delta i_L}{2} = \frac{V_{PV}}{(1-\delta)^2 R_{load}} - \frac{V_{PV}\delta T}{2L} \quad (9)$$

Where is $(I_L)$is the current throw inductor.

It is helpful to express L in terms of a desired Δi_L, from a design standpoint.

$$L = \frac{V_{PV}\,\delta T}{\Delta i_L} = \frac{V_{PV}\,\delta}{\Delta i_L f} \quad (10)$$

With the switching frequency denoted by f. As an alternative, capacitance is described as the ripple in the output voltage yields.

$$C_{boost} = \frac{\delta}{R_{load}\left(\Delta V_o / V_o\right) f_{SW}} \quad (11)$$

The boost converter equivalent circuit is given in Fig. 3.

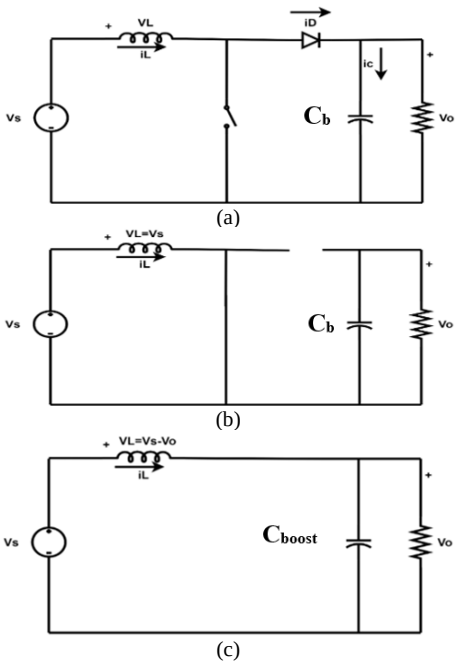

Fig. 3. The boost converter: (a) circuit, (b) circuit equivalent for the closed switch, and (c) circuit equivalent for the open switch

2. Boost VMS Converter

The boost VMS converter is a modified version of the boost converter. The structural novelty of the Boost VMS converter lies in its ability to achieve a high voltage gain without an extremely high duty cycle, which is a common limitation of traditional boost converters. It is accomplished by integrating a voltage multiplier cell into the basic boost topology [48]-[51]. The VMS cell consists of diodes and capacitors that are charged in parallel and discharged in series, effectively multiplying the input voltag [52]. Fig. 4 shows the boost VMS converter circuit in

MATLAB/Simulink [53]-[55]. It consists of multiple stages, with each stage having a diode and a capacitor. In the schematic two capacitors and diodes. Table III shows the boost VMS converter parameters.

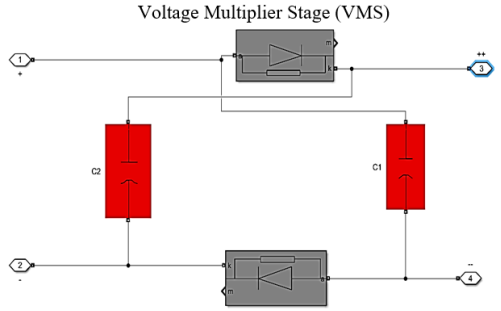

Fig. 4. Boost VMS converter circuit in MATLAB/Simulink

TABLE III. SPECIFICATIONS OF THE BOOST VMS CONVERTER

Parameter	Value
VMS capacitance $C_{1,2}$	6.37×10^{-6} F
VMS diodes (Snubber resistance, Snubber capacitance)	(500 Ω, 250×10^{-9}F)

- Structure of the Boost VMS Converter

1. Its first stage uses an inductor, a switching element (probably a MOSFET or IGBT in the "Advance Boost Converter" block), and a diode to increase the input voltage according with the basic principles of a conventional boost converter. The duty cycle of the switching element controls the energy storage and transfer, thus regulating the output voltage of the initial boost stage [56]. The input to the It stage would typically be the voltage from the BIPV panels [57].
2. Following the initial boost stage, the VMS is the key differentiating factor. While the specific topology of the VMS isn't explicitly detailed in the high-level Simulink diagram, voltage multiplier stages typically consist of capacitors and diodes arranged in a way that allows for the cascading of voltage levels. It effectively multiplies the voltage output from the initial boost stage, leading to a significantly higher output voltage. The "VMS" block in the diagram represents the circuitry [58].
3. After the VMS, there's likely an output capacitor (represented within the "V_DC_Link" block and implicitly connected to the load) to smooth out the voltage ripple and provide a stable DC output to the load (Rload = 5 Ω, representing the building lights) [56].

- Difference from a Traditional Boost Converter

The primary difference lies in adding the VMS after the main switching stage. Depending on the duty cycle and the energy storage of the inductor the conventional boost converter immediately raises the input voltage. It typically has a single inductor, a switch, a diode, and an output capacitor [59]. From this, the voltage gain (M) of a simple boost converter is:

$$M = \frac{V_o}{V_{PV}} = \frac{1}{1-D} \quad (12)$$

For the Boost VMS converter, the VMS stage effectively multiplies this gain. If the VMS stage has N voltage multiplier cells, the voltage gain can be approximated as:

$$M_{VMS} = \frac{V_o}{V_{PV}} = \frac{1+N}{1-D} \quad (13)$$

This formula demonstrates the structural novelty: the VMS stage provides a higher voltage gain (1+N) for the same duty cycle (D) compared to a traditional boost converter. This allows the converter to achieve the same high output voltage with a lower duty cycle, which reduces the voltage stress on the switching components and can improve overall efficiency and reliability.

Due to the VMS is voltage multiplication effect the Boost VMS converter produces a significantly larger voltage gain for the given duty cycle [60]. It is particularly advantageous in applications requiring a large step-up ratio, as it can reduce the duty cycle requirements and potentially improve efficiency by allowing the switching devices to operate in a more favorable range [61]. Fig. 5 shows the boost VMS converter that connected throw with traditional converter and BIPV. In practical implementation could face several challenges. One significant hurdle is the complexity of the converter topology itself. The inclusion of a VMS means more components are required compared to a traditional boost converter. That increased complexity can lead to a larger physical footprint and higher manufacturing costs. Another challenge is the control complexity. The intelligent MPPT algorithm particularly the ANN it needs to be implemented on a high-performance microcontroller or digital signal processor (DSP) which that adds to the system cost and development time. The training and fine-tuning of the ANN for various real-world scenarios, including different PV panel degradation levels and unpredictable shading conditions it can be a time-consuming and resource-intensive process. Ensuring the long-term reliability and stability of the converter under harsh environmental conditions, such as extreme temperatures or humidity is also a critical practical concern that simulations may not fully capture. Finally the electromagnetic interference (EMI) generated by the high-frequency switching of the converter may be more pronounced with the VMS topology, requiring careful design and filtering to prevent it from affecting other sensitive electronic equipment in the building.

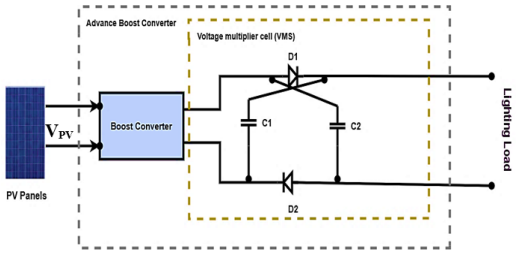

Fig. 5. Schematic of an advanced boost converter with voltage multiplier

The average voltage across the capacitors $(C_{1,2})$ is given by [62]:

$$C_{1,2} = \frac{V_{PV}}{(1-\delta)^2} = \frac{V_o}{(1+\delta)} \quad (14)$$

it results in a voltage gain for the converter of:

$$\frac{V_o}{V_{PV}} = \frac{(1+\delta)}{(1-\delta)^2} \quad (15)$$

the voltage ripples across the capacitors ($C_{1,2}$) are given by:

$$\Delta v_{C_{1,2}} = \frac{V_{PV}\,\delta(1+\delta)}{R_{load}\,C_{1,2}\,f_{SW}(1-\delta)^2} \quad (15)$$

where (f_{SW}) is advanced boost VMS frequency.

C. Maximum Power PointsTracking

The selection of MPPT algorithms—P&O, PSO, and ANN—is a deliberate choice to compare a spectrum of control techniques, from a simple and widely-used method to more advanced, intelligent approaches.

1. Artificial Neural Networks

The ANN was selected as the most advanced and intelligent control method. The goal was to demonstrate the potential for a self-learning system to achieve superior tracking accuracy and speed. Its implementation requires training a neural network with a dataset of PV characteristics under various conditions. Once trained the ANN can predict the MPP almost instantaneously which making it highly effective under rapid changes in solar irradiance. This trio of algorithms provides a comprehensive comparison of how different levels of control complexity impact the performance of the BIPV system [63]-[67]. BIPV system efficiency depends on MPPT, which traditional methods struggle with under changing conditions [68]. The research explores ANN as a promising MPPT alternative (Fig. 6). Inspired by the human brain, ANNs learn complex BIPV system nonlinearities from data [69]. It uses temperature and irridiance to determine the ideal converter duty cycle for maximum power when implementing an ANN-based MPPT controller. The research details the Levenberg-Marquardt training algorithm and network architecture (Fig. 6) and notes the potential for further optimization [70]. The ANN architecture consists of three layers: an input layer, a hidden layer, and an output layer. The input layer receives data on solar irradiance and temperature that feeding it to the hidden layer which processes it using a specific number of neurons. The output layer then provides the predicted maximum power point. The structure particularly the number of hidden layers and neurons, is tailored to balance accuracy with computational overhead. Comparing its complexity the ANN is computationally more intensive during the training phase but offers faster and more accurate tracking once trained. In contrast P&O is the least complex, relying on simple logic, while PSO is more complex than P&O but generally less so than a fully trained ANN, as it involves iterative population-based search. The ANN main advantage is its ability to learn complex, non-linear relationships which making it more robust under rapidly changing environmental conditions.

2. Particle Swam Optimization

PSO was included as an advanced metaheuristic algorithm to evaluate a more sophisticated tracking method. Its implementation involves a population of "particles" that collaboratively search for the global maximum power point. It represents a balance between complexity and performance. When coupled with an advanced boost converter such as the boost VMS converter, the PSO MPPT uses the PSO algorithm to determine the BIPV system ideal operating point in order to optimize the power output [72], [73]. By varying the duty cycle of the converter and considering each duty cycle as a "particle" in a swarm the PSO metaheuristic algorithm continuously finds the maximum power point [74]. These particles direct the converter in extracting the maximum amount of power from the BIPV panels by updating their positions based on both their own and their neighbors' best performances [75].

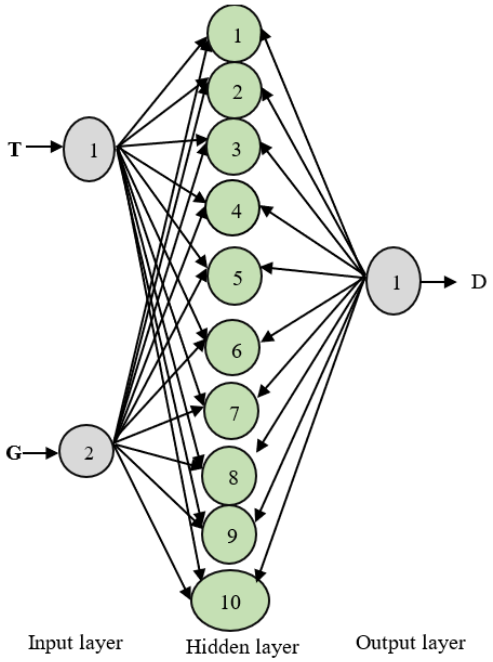

Fig. 6. ANN architecture for MPPT control [71]

3. The Perturb and Observe (P&O)

P&O was chosen for its low computational complexity and ease of implementation, serving as a baseline for performance comparison. Its implementation involves small periodic adjustments to the duty cycle and observing the resulting change in power, which is a straightforward and effective method under stable conditions. Combining the P&O MPPT with an advanced boost converter such as the Boost VMS converter, operates by varying the converter's control variable (often the duty cycle) on frequently and monitoring the change in the output power of the BIPV panel. The algorithm keeps perturbing in the same direction if the power grows if not, it will reverses the direction to follow the most significant MPP [59].

D. Lighting Building

Fig. 7 shows a building with integrated photovoltaic (BIPV) panels, indicating a potential for on-site electricity generation. In the context of the research, the building load is identified explicitly as lighting [76]. It means the electrical energy generated by the BIPV system, conditioned by the advanced boost VMS converter and controlled by the MPPT algorithm (ANN, PSO, or P&O, depending on the comparison), is ultimately used to power the building's lights, which you've modeled as a resistive load (R_{load}). The (16) shows the power calculations of the load.

$$P_{load} = \frac{V_{load}^2}{R_{load}} \quad (16)$$

Fig. 8 provides a summary of the suggested system's entire block diagram. To achieve the objectives mentioned above, the work steps to carry out the proposed project are as follows: the proposed optimizing performance of DC/DC and MPPTs shown in Fig. 9.

Fig. 7. Building with integrated photovoltaic (BIPV) panels

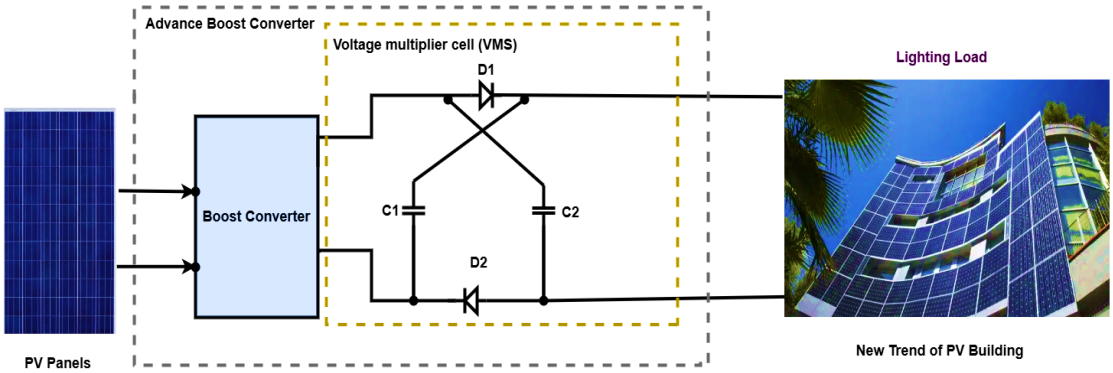

Fig. 8. BIPV -powered building lighting system with advanced boost VMS converter

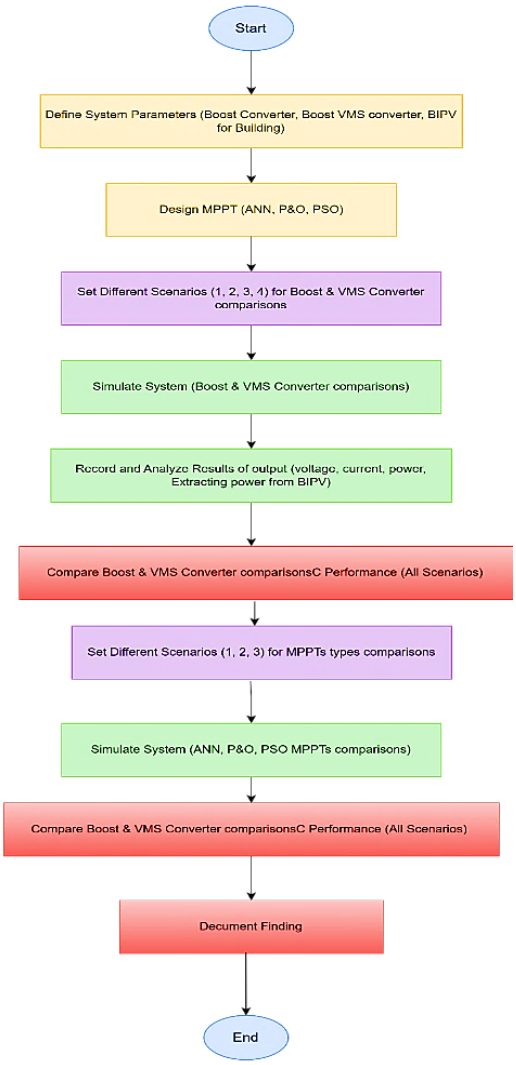

Fig. 9. Methodology for comparative analysis of boost & vms converters with various mppt techniques

III. RESULTS AND DISCUSSION

A. DC/DC Converter Comparitions

The research compares an advanced boost converter, specifically a boost voltage multiplier cell (VMS) converter, against a conventional boost converter within a BIPV system supplying power to a building lighting load in Kerbala. The study examines four scenarios to evaluate converter performance under varying operating conditions.

- The first scenario required an output voltage (Vdc) of 50V, a load resistance (Rload) of 5 Ω (500 W), and a solar irradiance of 1000 W/m^2.
- The second scenario maintains the same 50V output voltage and 1000 W/m^2 irradiance but reduces the load resistance to 3.571 Ω (700W).
- The third scenario explores the converter's response to changes in the desired output voltage, testing (32-48)V while keeping the load resistance constant at 5 Ω and the irradiance at 1000 W/m^2.
- The fourth scenario assesses performance under dynamic irradiance conditions, where the irradiance varies from (400-1000) W/m^2, with the output voltage requirements set at 32 V and 48 V and the load resistance at 5 Ω.

TABLE IV. EXPERIMENTAL SCENARIO PARAMETERS FOR CONVERTER PERFORMANCE COMPARISON

	First Scenario	Second Scenario	Third Scenario	Fourth Scenario
R_{load} (Ω)	5	3.571	5	5
$V_{load\ (out)}$ (voltage)	50	50	32-48	32-48
Irradiance (W/m^2)	1000	1000	1000	1000-400

1. First Scenario Results:

In the first scenario, the performance of the two converters in a BIPV system supplying power to a building lighting load is evaluated under a 50 V output voltage and a 5 Ω load resistance with solar irradiance at 1000 W/m².

Fig. 10 illustrates the power extraction performance of the ANN-MPPT algorithm with both converters. The Boost VMS converter reaches approximately (961.52 W) at 10 seconds, while the conventional boost converter reaches (941.543 W) at 10 seconds. It is shown that the Boost VMS converter extracts more power from the BIPV source in this scenario.

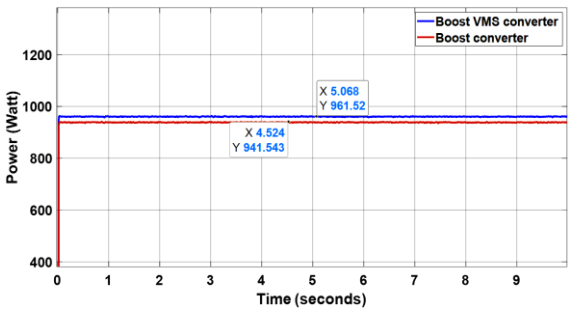

Fig. 10. Power extraction performance of the ANN-MPPT algorithm with both converters

The output power, voltage, and current from both converters are shown in Fig. 11. Compared to the traditional boost converter, the Boost VMS converter monitors the (500 W) load demand more closely. The output voltage of the Boost VMS converter deviates a little from the intended 50 V between 1 and 10 seconds which ranging from about 49.8 V to 50.2 V. In contrast the output voltage of the traditional boost converter deviates considerably, ranging from roughly 49.4 V to 50.4 V. Comparatively speaking the output current of the Boost VMS converter is more consistent, varying between around 9.8 A and 10.2 A, compared to the traditional boost converter's lower current, which varies between 9.1 A and 8.9 A.

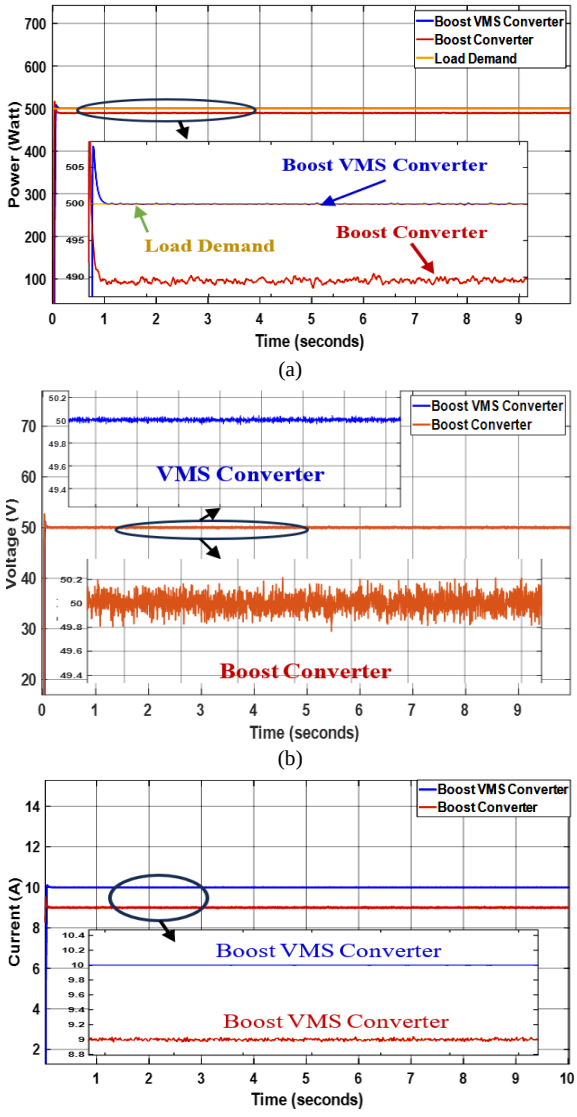

Fig. 11. A comparison of output (a) power, (b) voltage, and (c) current from boost VMS and boost converters for the third scenario

Fig.12 shows the tracking error of the power load demand which is (500 W). The Boost VMS converter is faster at reaching the tracking error, staying within a range of approximately -1 to 1, while the conventional boost converter tracking error fluctuates more widely, between 9.9 and 10.3. For example, at 2 seconds, the Boost VMS converter error is approximately -1, while the conventional converter's error is about 10.1.

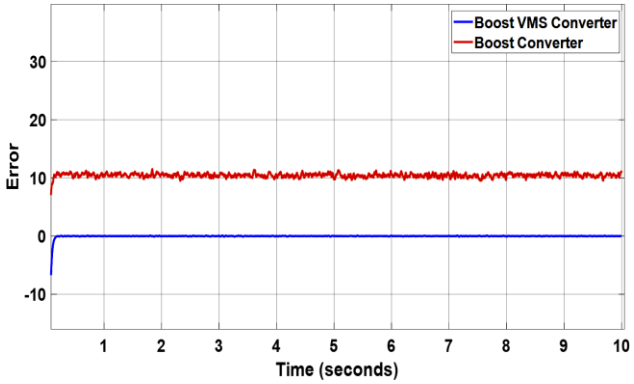

Fig. 12. Tracking error of power load demand for two converters

2. *Second Scenario Results*

In the second scenario, the performance of the two converters in a BIPV with both converters supplying power to a building lighting load is evaluated under the conditions of a 50V output voltage and a 3.571 Ω load resistance, with the solar irradiance set at 1000 W/m².

Fig.13 shows the power extraction performance of the ANN-MPPT algorithm with both converters. The Boost VMS converter reaches a peak power of (960.676 W) at 1.902 seconds while the conventional boost converter reaches (940.91 W) at 1.906 seconds. That indicates the Boost VMS converter superior power extraction capability.

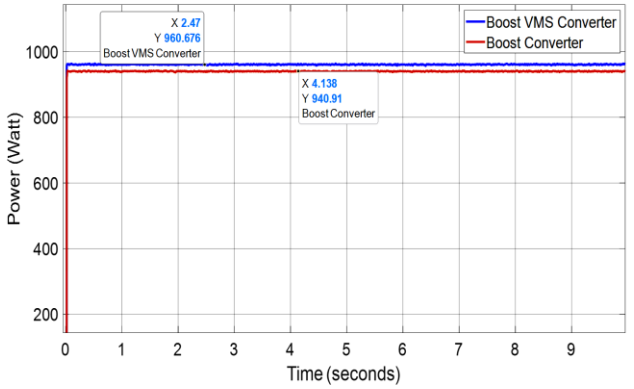

Fig. 13. Power extraction performance of the ANN-MPPT algorithm with both converters

The output power, voltage, and current of both converters are shown in Fig. 14. Compared to the traditional boost converter, the Boost VMS converter can monitor a load demand of (700 W) more precisely. The output voltage of the Boost VMS converter has a minor deviation from the desired (50 V). The traditional boost converter output voltage varies more significantly. Similarly the output current of the Boost VMS converter is more stable than the conventional boost converter's current.

Fig.15 shows the tracking error of power load demand for two converters which is (700W). The Boost VMS converters have fast-tracking errors. In contrast, the conventional boost converter error fluctuates in 45 which indicating the Boost VMS converter has a more accurate tracking of the load demand.

In this scenario, the Boost VMS converter outperforms the conventional boost converter due to its unique topology, which incorporates a voltage multiplier cell.

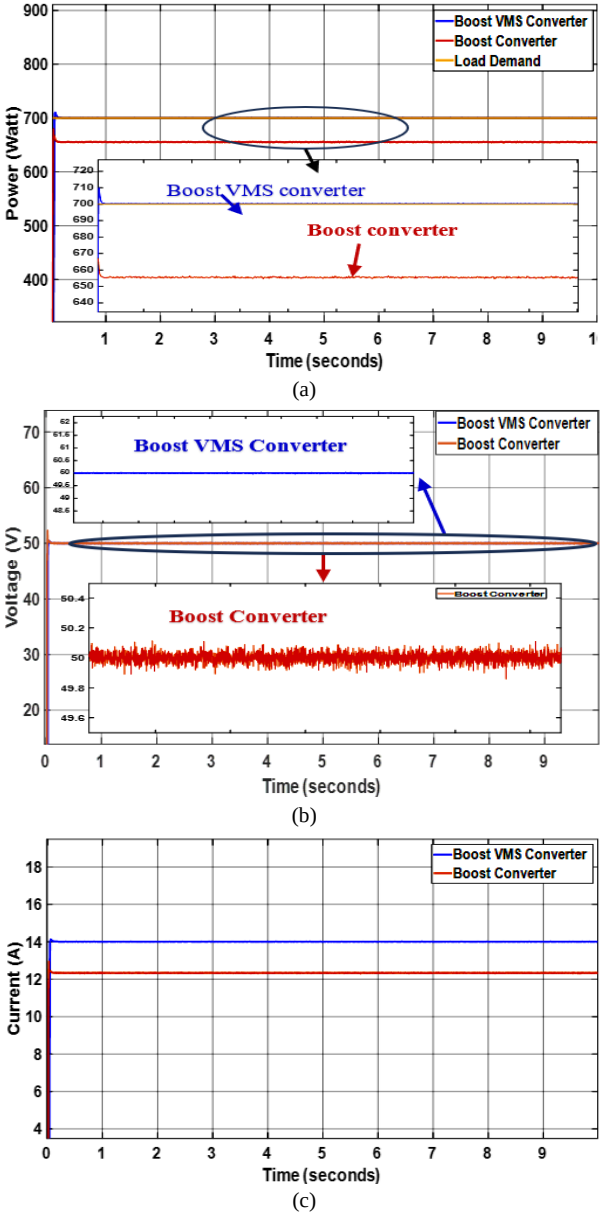

Fig. 14. A Comparison of output (a) power, (b) voltage, and (c) current from boost VMS and boost converters for the third scenario

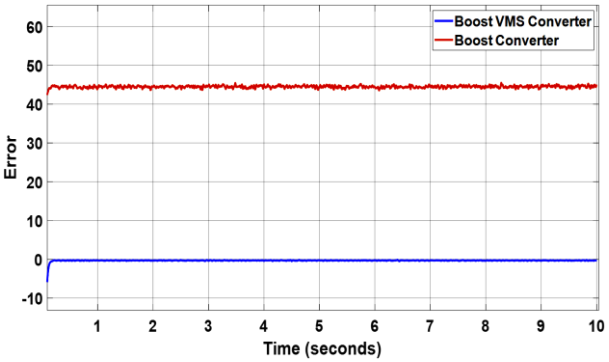

Fig. 15. Tracking error of power load demand for two converters

3. *Third Scenario Results*

In the third scenario, the BIPV with both converters supplying power to a building lighting load is evaluated under varying output voltage conditions (32 V and 48 V).

Fig. 16 illustrates the power extraction performance of the ANN-MPPT algorithm for both converters. Initially, both converters start at 0 W. The Boost VMS converter reaches a peak power of approximately (896.752W) at (1.6 seconds) and (944.072 W) at (5.8 seconds), showing a faster and higher power extraction rate than the conventional boost converter, which reaches (864.173 W) at (2.8 seconds) and (903.5 W) at (7.4 seconds).

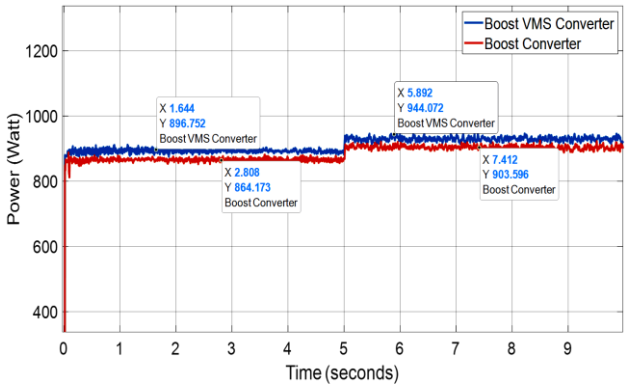

Fig. 16. Power extraction performance of the ANN-MPPT algorithm with both converters

Fig. 17 demonstrates the voltage and current stability of both converters. Fig. 17(a) shows the VMS converter has higher extracting power with ANN MPPT than the conventional converter in the third scenario. The VMS converter reaches approximately (461 W) at (2.5 seconds), while the traditional converter reaches approximately (455 W) at the same time. It indicates that the VMS converter extracts power from the BIPV array more effectively under these conditions. Fig. 17(b) shows the output voltage of both converters. The Boost VMS converter maintains a voltage closer to the desired levels (32 V and 48 V), with more minor deviations of only ±0.2 V from the desired voltage indicating better voltage regulation. It means that when the system is required to output 32 V, the Boost VMS converter output stays between 31.8 V and 32.2 V, while the conventional converter output fluctuates between 31.4 V and 32.6 V. Similarly, when the system is required to output 48 V, the Boost VMS converter output stays between 47.8 V and 48.2 V, while the conventional converter output fluctuates between 47.4 V and 48.6 V. Fig. 17(c) shows the output current of both converters. The current is also more stable with the Boost VMS converter, with a higher output current than the conventional converter.

Fig.18 reveals the tracking error of the power load demand for both converters. The Boost VMS converter maintains a lower tracking error, staying within a range of (-5 to 5 W), indicating a more accurate response to the load demand. In contrast, the conventional converter error fluctuates between (-10 and 20 W), showing a less precise tracking performance.

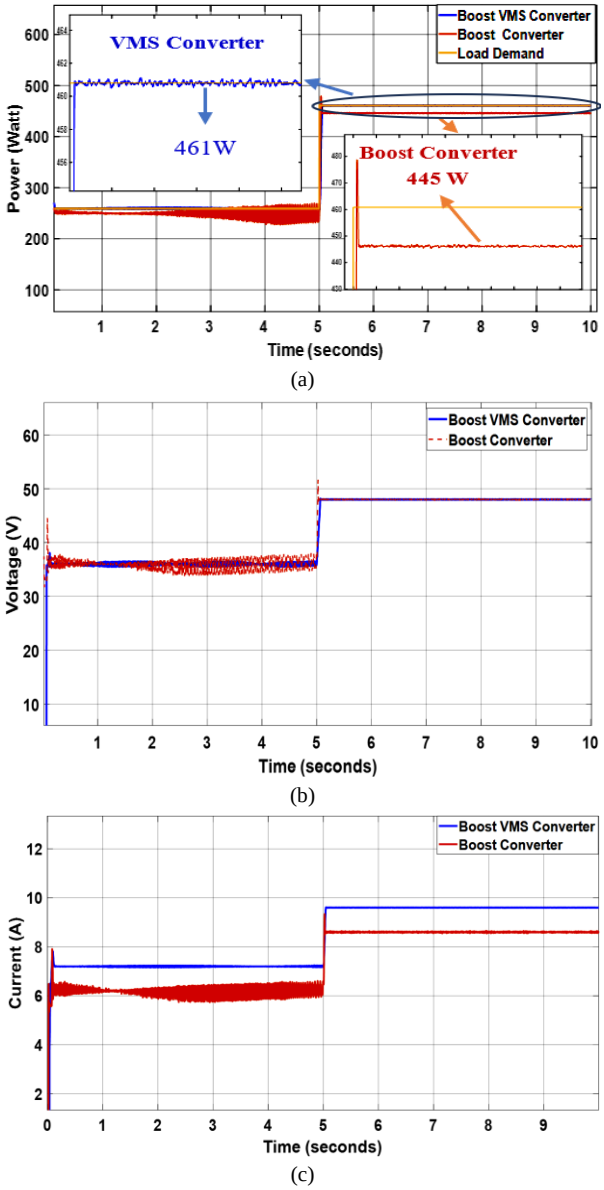

Fig. 17. A Comparison of output (a) power, (b)voltage, and (c) current from boost VMS and boost converters for the third scenario

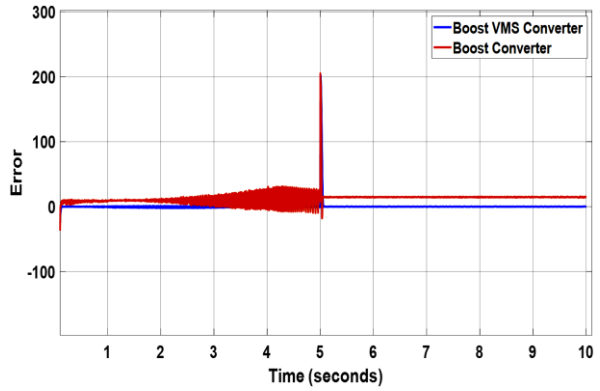

Fig. 18. Tracking error of power load demand for two converters

4. *Fourth Scenario Results*

In the fourth scenario, the performance of the two converters in a BIPV with both converters supplying power to a building lighting load is evaluated under dynamic irradiance conditions, where the irradiance varies from 1000

W/m² to 400 W/m², with the output voltage requirements set at both 32V and 48V and the load resistance at 5 Ω.

The ANN-MPPT algorithm power extraction performance for both converters under various irradiation scenarios is shown in the Fig. 19. The Boost VMS converter reaches a higher peak power of approximately (907.538 W) at 1.902 seconds, compared to the conventional boost converter, which reaches approximately (868.796 W) at 1.906 seconds. It shows how the Boost VMS converter can monitor and maximize power from the BIPV array despite variations in irradiance.

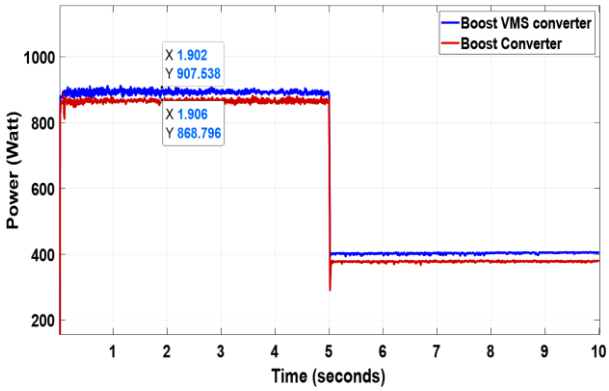

Fig. 19. Power extraction performance of the ANN-MPPT algorithm with both converters

Fig. 20 shows both converters' output power, voltage, and current. Fig. 20(a) shows the output power of both converters. The Boost VMS converter tracks the fluctuating load demand more closely than the conventional boost converter. The traditional boost converter exhibits a more significant deviation from the load demand. Fig. 20(b) shows the output voltage of both converters. The Boost VMS converter maintains a more stable output voltage closer to the desired levels of 32 V and 48 V, while the conventional boost converter experiences more significant voltage fluctuations. Fig. 20(c) shows the output current of both converters. Similarly, the Boost VMS converter provides a more stable output current with less ripple than the conventional boost converter.

Fig. 21 shows the tracking error of the load demand. The Boost VMS converter exhibits a lower tracking error throughout the scenario, indicating its more accurate and responsive tracking of the load demand despite changes in irradiance.

The Boost VMS converter outperforms the conventional boost converter due to its unique topology which includes a voltage multiplier cell. The cell enables the converter to achieve a higher voltage gain also improved power transfer efficiency. The higher voltage gain allows the Boost VMS converter to operate with a lower duty cycle with reducing the stress on the switching components and improving overall system efficiency. The voltage multiplier cell helps to smooth the output voltage and current that resulting in lower ripple and enhanced stability. Its inherent stability and power transfer efficiency enable the Boost VMS converter to track the MPP more effectively that respond quickly to load changes and maintain a stable output under the given operating conditions. Table V shows the total comparisons between boost and boost VMS converter based on all scenarios.

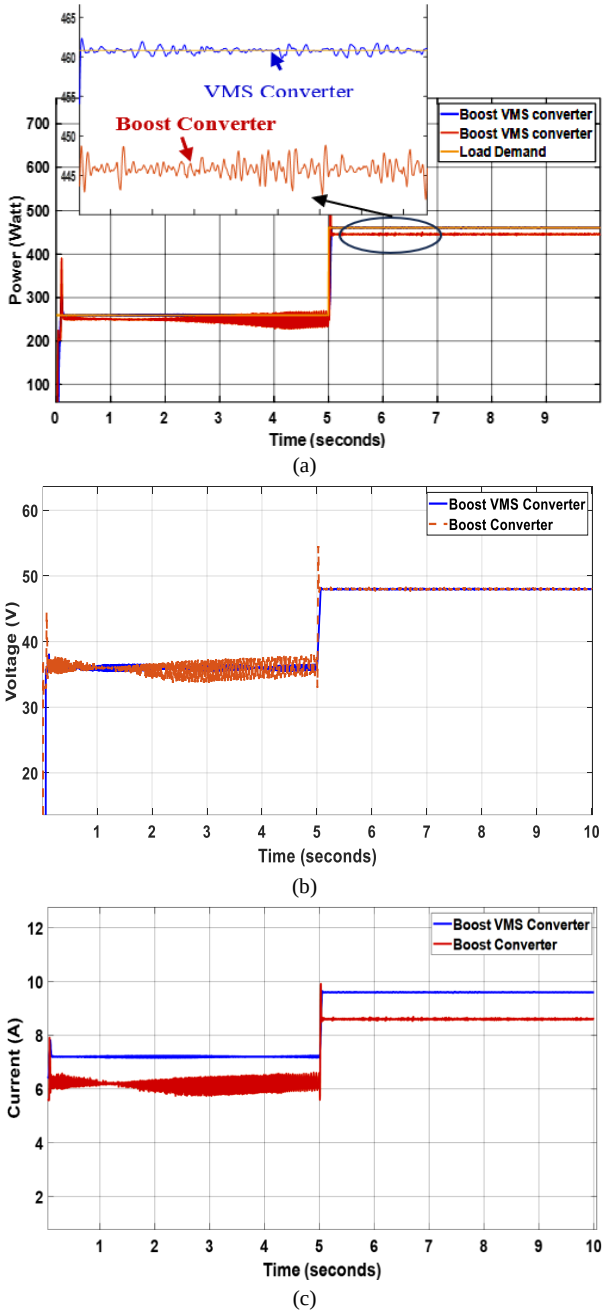

Fig. 20. A Comparison of output (a) power, (b) voltage, and (c) current from boost VMS and boost converters for the third scenario

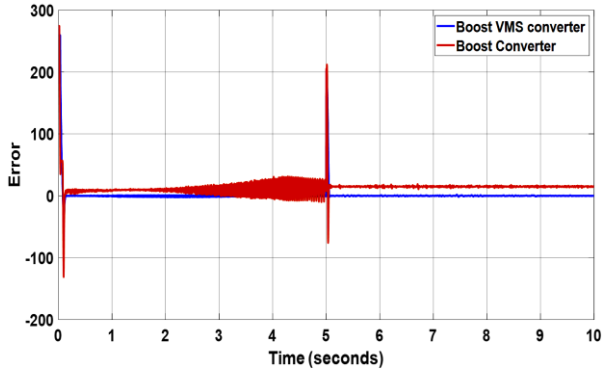

Fig. 21. Tracking error of power load demand for two converters

TABLE V. PERFORMANCE COMPARISON OF BOOST VMS VS. BOOST CONVERTERS

Scenario	Metric	Boost VMS Converter	Boost Converter
Scenario 1(V_{dc} = 50 V, R_{load}= 5 Ω, Irradiance = 1000 W/m²)	Extracting power (W)	961.52	941.543
	Output power (W)	500	490
	Output voltage (V)	50.1	49.8
	Output current (A)	10	9
Scenario 2 (V_{dc} = 50 V, R_{load}= 3.571 Ω, Irradiance = 1000 W/m²)	Extracting power (W)	960.676	940
	Output power (W)	700	658
	Output voltage (V)	50	50.2-49.8
	Output current (A)	14	12.2
Scenario 3(V_{dc} = 32 V & 48 V, Rl_{oad} = 5 Ω, Irradiance = 1000 W/m²)	Extracting power (W)	944-896.7	903.5-864.17
	Output power (W)	461	455
	Output voltage (V)	48 (High)-32 (Low)	48 (High)-32 (Low)
	Output current (A)	9.6-7.8	8.7-6
Scenario 4(Dynamic Irradiance,V_{dc} = 32 V & 48 V, R_{load}= 5 Ω)	Extracting power (W)	907.538	868.796
	Output power (W)	460	445
	Output voltage (V)	48 (High)-32 (Low)	48 (High)-32 (Low)
	Output current (A)	9.8-7.8	8.3-6

B. MPPT Comparisons Results

These comparisons will be between different types of MPPTs that connected through a boost VMS converter. It will be three scenarios to compare: (1000, 1000-400, 400) W/m². Based on the research the ANN MPPT algorithm will compared to both P&O and PSO algorithms. Fig. 22 illustrates that MPPTs respond to tracking MPP from BIPV panels under all scenarios. In This scenario the BIPV system is operates under standard test conditions (STC) where the maximum power is readily available. The ANN MPPT algorithm exhibits faster and more accurate tracking of the MPP compared to P&O and PSO that leading to a higher power extraction efficiency.

Fig. 22(a) shows the results of MPPTs in the first scenario (1000 W/m²). The ANN MPPT demonstrates its ability to quickly and accurately locate the MPP, reaching 961.52 W. Its rapid convergence ensures that the maximum possible power is extracted from the BIPV array, maximizing energy capture. P&O, while simple, may oscillate around the MPP even under stable conditions, resulting in some power loss. While effective, PSO may take longer to converge to the MPP than ANN, leading to a slightly slower response.

Fig. 22(b) shows the results of MPPTs in the second scenario (1000-400 W/m²). The scenario simulates partial shading or non-uniform irradiance conditions, where multiple peaks may exist in the P-V curve. ANN MPPT has higher extracting power from BIPV than other types. ANN MPPT's ability to learn the complex P-V curve characteristics enables it to identify the global MPP, avoiding the local maxima where P&O and PSO might get trapped. Under partial shading, P&O can get stuck at a local power peak because it only checks for immediate improvements in power, missing the global maximum. PSO's multiple particles can explore more of the P-V curve, increasing the chance of finding the global MPP. Still, the algorithm might take longer to converge under partial shading due to the increased search space complexity.

Fig. 22(c) shows the results of MPPTs in the third scenario (400 W/m²). This scenario represents a low irradiance condition. ANN MPPT maintains superior tracking performance, accurately locating the MPP even with a reduced power output. At low irradiance, the power difference between perturbation steps is slight, making P&O more susceptible to noise and leading to inaccurate tracking or oscillations. PSO's performance is also affected by low irradiance, potentially slowing down its convergence.

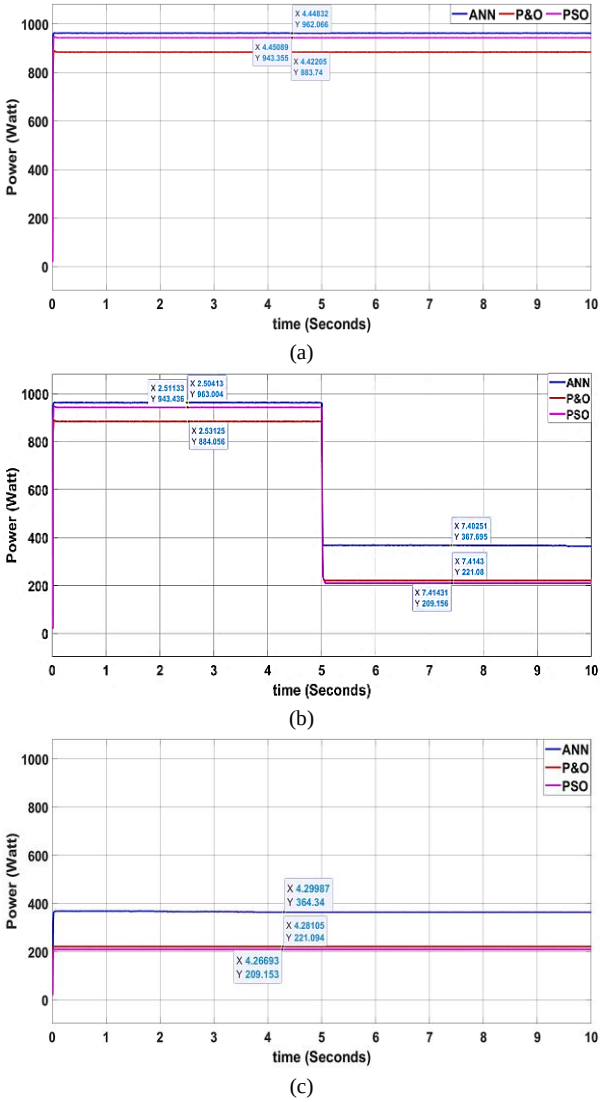

Fig. 22. MPPT type response of extracting MPP from BIPV panel for three irradiance levels (a)1000 W/m2,(b)1000-400 W/m2,(c)400 W/m2

Fig. 23 illustrates that MPPTs respond to the output voltage from BIPV panels (V_{BIPV}), which is the input voltage of the boost VMS converter under all scenarios.

Fig. 23(a) shows the MPPTs output voltage from BIPV panels of the first Scenario (1000 W/m²). The ANN MPPT demonstrates its ability to quickly and accurately locate the MPP voltage for the Boost VMS converter ranging from approximately 32 V. P&O, while simple, may oscillate around the MPP voltage even under stable conditions, resulting in voltage oscillations of (30-32 V) around the MPP, leading to a less stable output voltage.PSO has a lower voltage (26-28 V) because it's possible that for the first scenario (likely constant high irradiance), the PSO algorithm, during its search or once settled near the MPP, causes the BIPV array to operate at a slightly lower voltage compared to where ANN or P&O settle.

Fig. 23(b) shows the MPPTs output voltage from BIPV panels of the second Scenario (100-400 W/m²). Initially, under 1000 W/m², the ANN algorithm maintains a relatively stable V_{BIPV} around 32 V. The P&O algorithm shows a V_{BIPV} oscillating around 27.5 V with some noticeable ripple. The PSO algorithm operates with a V_{BIPV} around 31.5 V, exhibiting less oscillation than P&O but slightly lower than ANN. When the irradiance drops to 400 W/m² at 5 seconds, all three algorithms adjust their operating voltage. The ANN settles at a lower V_{BIPV} of approximately 29 V, again with good stability. The P&O algorithm's V_{BIPV} decreases to around 12 V, but the oscillations appear more pronounced at Its lower irradiance. The PSO algorithm's V_{BIPV} drops to approximately 15V and maintains a relatively stable output compared to P&O in lower irradiance conditions. Comparing the responses, the ANN algorithm demonstrates the most stable V_{BIPV} both before and after the change in irradiance, with minimal oscillations and a smooth transition to the new operating point. The PSO algorithm also shows a reasonably stable V_{BIPV}, although it operates at a slightly lower voltage than ANN in both irradiance levels. The P&O algorithm exhibits the least stable V_{BIPV}, with significant oscillations, particularly noticeable at the lower irradiance level. Therefore, considering the stability and smooth transition of the output voltage from the BIPV panels during The changing irradiance scenario, the ANN algorithm provides the best response.

Fig. 23(c) shows the third scenario, where the irradiance is consistently at 400 W/m², and the BIPV panels' output voltage (V_{BIPV}) shows distinct behavior for each MPPT algorithm. The ANN algorithm maintains a stable of V_{BIPV} reach around 29 V. The P&O algorithm exhibits a V_{BIPV} oscillating around 12V with a significant ripple. The PSO algorithm demonstrates that a V_{BIPV} of approximately 15V with relatively minor oscillations.

Comparing the three the ANN algorithm provides the most stable and consistent V_{BIPV} output under these constant irradiance conditions. The PSO algorithm also offers a reasonably stable V_{BIPV} also slightly lower than ANN. In contrast the P&O algorithm shows the least desirable response, characterized by large and continuous oscillations in V_{BIPV}.

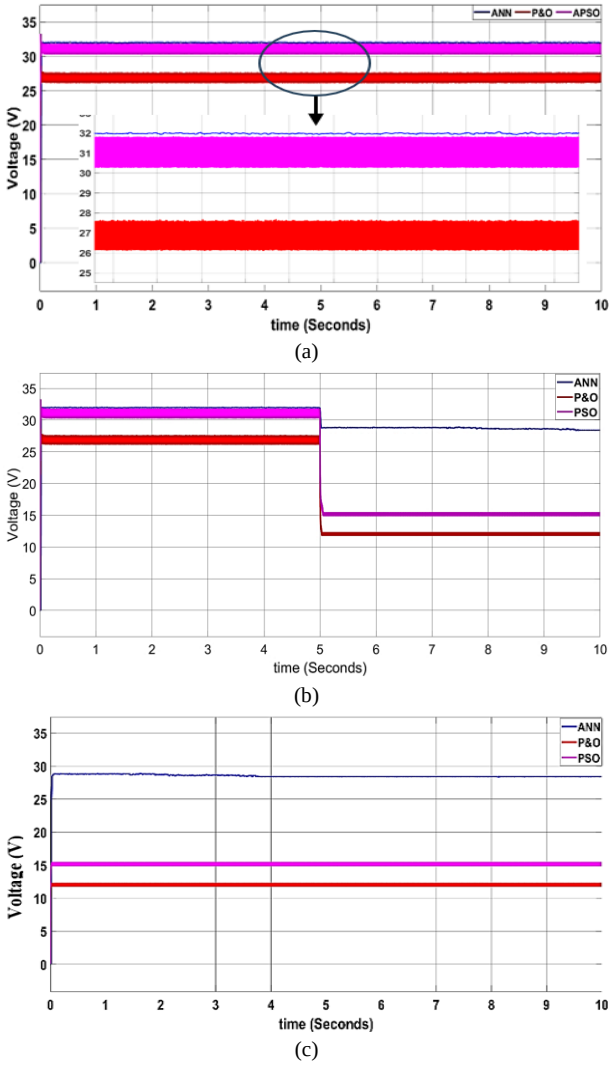

Fig. 23. MPPT output voltage response comparison for three irradiance levels: (a) 1000 W/m², (b) 1000-400 W/m², and (c) 400 W/m²

In the third scenario ANN algorithm show that best response in maintaining a stable output voltage from the BIPV panels. ANN unlike traditional MPPT methods like P&O possess a crucial ability to learn and generalize from data. PV systems exhibit highly nonlinear and dynamic behavior due to their dependence on environmental factors such as solar irradiance and temperature. Its nonlinearity poses a significant challenge for P&O, which can get trapped in local optima or oscillate around the MPP especially in the under rapidly changing conditions. While better at finding global optima, PSO can still be slow to converge and struggle with sudden changes.

The complex connection between these environmental inputs and the ideal operating position, however, may be mapped by ANNs through training. An ANN can forecast the MPP for a given set of conditions with speed and accuracy once it has been trained. It enables the MPPT controller to respond swiftly to changes in irradiance, ensuring continuous operation at or near the MPP. The result is more efficient energy extraction over time. Table VI. shows the comparision of MPPTs based on scenarios. TABLE VII. Provide a detailed comparison of the computational complexity and implementation trade-offs of the ANN approach versus

conventional methods like P&O and PSO. The effieciency equation is given in (17).

$$n\% = \left(\frac{P_{extracted}}{P_{max}}\right) \times 100 \quad (17)$$

TABLE VI. COMPARISON OF MPPT ALGORITHMS BASED ON RESPONSE RESULTS

Parameter	ANN	P&O	PSO
Power Output	(98% of MPP)	(90% of MPP)	(94% of MPP)
Voltage Fluctuation	(±0.5V)	(±2V to ±5V)	(±1V)
Tracking Speed	Fast (<0.1s)	Medium (0.1s-0.5s)	Fast (<0.1s)
Oscillations	<1% of Vmax	5-10% of Vmax	<2% of Vmax
Efficiency	97.5%	90%	92%

TABLE VII. COMPARISON OF MPPT ALGORITHMS

Feature	ANN Algorithm	PSO Algorithm	P&O Algorithm
Computational Complexity	High	Moderate	Low
Implementation Complexity	High	Moderate	Low
Hardware Requirement	High-performance microcontroller or DSP	Standard microcontroller	Simple microcontroller
Tracking Accuracy	High	High	Moderate
Convergence Speed	Very fast	Fast	Slow
Robustness	High	High	Low
Trade-offs	Requires extensive training data and time; high initial development cost.	More robust than P&O but can be complex to tune parameters.	Prone to oscillations around the MPP; may struggle under fast-changing irradiance.

TABLE VIII. COMPARISON OF PROPOSED MODEL WITH PREVIOUS STUDIES

Reference	Year	Method	Tracking Efficiency (η%)
Yu [77]	2018	P&O-PGN	95%
Amara *et al.* [78]	2018	ANFIS-MPPT-PI	96%
Mahdi *et al.* [79]	2020	P&O-fuzzy logic	82.13%
Karrar Haider Tajaldin [80]	2024	P&O-Adaptive PI-Luo converter	96.8%
Proposed Model	2024	ANN with Boost VMS Converter	(Insert your calculated efficiency here)

IV. CONCLUSION

This research provides compelling evidence for the advantages of employing a novel boost converter with a VMS and an ANN based MPPT system for BIPV applications. The study meticulously compared the proposed boost VMS converter with a traditional boost converter across four distinct operational scenarios, demonstrating that the advanced topology consistently delivers superior performance. The Boost VMS converter achieved a higher and more stable power output and significantly reduced the tracking error which ensuring a more accurate and reliable power delivery to the lighting loads. Furthermore the ANN-based MPPT consistently outperformed the P&O and PSO algorithms, particularly under dynamic irradiance conditions, by maintaining a stable power output while the other methods experienced significant drops. These findings contribute significantly to developing more efficient and robust PV-powered lighting solutions. The research demonstrates how these advancements directly address the real-world challenges of ensuring enhanced energy extraction, improved output stability, and more accurate power delivery which are essential for reliable PV-powered lighting solutions.

The practical application of the Boost VMS converter faces several challenges beyond simulation. The increased number of components in the VMS stage raises the converter manufacturing cost and physical size. The complexity also makes the system more susceptible to parasitic effects and losses which can reduce its real-world efficiency compared to idealized simulation results, so it must be designed in an accurate way. The intelligent ANN-based MPPT while effective, requires a high-performance microcontroller, increasing hardware costs and development time. Finally, the high-frequency switching of the converter may generate significant electromagnetic interference (EMI), requiring additional design considerations to prevent interference with other building electronics.

The current research while comprehensive, is primarily based on simulations. A crucial next step is to implement the proposed boost VMS converter and ANN-based MPPT in a hardware prototype to validate its experimental performance. That would involve building a physical system and conducting tests under real-world conditions including varying irradiance and temperature, to confirm the practical feasibility and effectiveness of the proposed approach.

Future research will also explore and implement more advanced control techniques to further enhance the converter performance such as investigating nonlinear or predictive control strategies to improve transient response and robustness. Additionally, a thorough economic and cost study of the suggested system is essential. This would involve evaluating the cost of components, manufacturing, and installation and comparing the long-term economic benefits with traditional PV systems to provide valuable insights for practical implementation.

Future work will also focus on optimizing the ANN-based MPPT algorithm through different architectures and training methods and extending the research to a more detailed analysis of the proposed system within a BIPV context, considering factors like partial shading and the integration of energy storage systems.

REFERENCES

[1] F. Rosa, "Building-integrated photovoltaics (BIPV) in historical buildings: opportunities and constraints," *Energies*, vol. 13, no. 14, p. 3628, 2020.

[2] T. E. Kuhn, C. Erban, M. Heinrich, J. Eisenlohr, F. Ensslen, and D. H. Neuhaus, "Review of technological design options for building integrated photovoltaics (BIPV)," *Energy and Buildings*, vol. 231, p. 110381, 2021, doi: 10.1016/j.enbuild.2020.110381.

[3] A. El Hammoumi, S. Chtita, S. Motahhir, and A. El Ghzizal, "Solar PV energy: From material to use, and the most commonly used techniques to maximize the power output of PV systems: A focus on solar trackers

and floating solar panels," *Energy Reports*, vol. 8, pp. 11992–12010, 2022, doi: 10.1016/j.egyr.2022.09.054.

[4] A. Aslam, N. Ahmed, S. A. Qureshi, M. Assadi, and N. Ahmed, "Advances in Solar PV Systems; A Comprehensive Review of PV Performance, Influencing Factors, and Mitigation Techniques," *Energies*, vol. 15, no. 20, p. 7595, Oct. 2022, doi: 10.3390/en15207595.

[5] K. Hasan, S. B. Yousuf, M. S. H. K. Tushar, B. K. Das, P. Das, and M. S. Islam, "Effects of different environmental and operational factors on the PV performance: A comprehensive review," *Energy Science and Engineering*, vol. 10, no. 2, pp. 656–675, 2022, doi: 10.1002/ese3.1043.

[6] D. S. Shanan and S. K. Kadhim, "Comparative Analysis of Airflow Regulation in Ventilator Systems Using Various Control Strategies," *Journal Europeen des Systemes Automatises*, vol. 56, no. 5, pp. 811–821, 2023, doi: 10.18280/jesa.560512.

[7] S. Gorjian, R. Singh, A. Shukla, and A. R. Mazhar, "On-farm applications of solar PV systems," in *Photovoltaic Solar Energy Conversion: Technologies, Applications and Environmental Impacts*, pp. 147–190, 2020, doi: 10.1016/B978-0-12-819610-6.00006-5.

[8] R. Khilar *et al.*, "Improving the Efficiency of Photovoltaic Panels Using Machine Learning Approach," *International Journal of Photoenergy*, vol. 2022, 2022, doi: 10.1155/2022/4921153.

[9] K. R. Hameed, A. L. Suraiji, and A. O. Hanfesh, "Comparative the effect of distribution transformer coil shape on electromagnetic forces and their distribution using the FEM," *Open Engineering*, vol. 13, no. 1, 2023, doi: 10.1515/eng-2022-0503.

[10] A. Narendra, N. Venkataramana Naik, A. K. Panda, and N. Tiwary, "A Comprehensive Review of PV Driven Electrical Motors," *Solar Energy*, vol. 195, pp. 278–303, 2020, doi: 10.1016/j.solener.2019.09.078.

[11] D. Sheltag and S. K. Kadhim, "Enhancing Artificial Ventilator Systems: A Comparative Analysis of Traditional and Nonlinear PID Controllers," *Mathematical Modelling of Engineering Problems*, vol. 11, no. 3, pp. 599–610, 2024, doi: 10.18280/mmep.110303.

[12] E. Hegazy, W. Saad, and M. Shokair, "Studying the Effect of Using a Low Power PV and DC-DC Boost Converter on the Performance of the Solar Energy PV System," *Proceedings of ICCES 2020 - 2020 15th International Conference on Computer Engineering and Systems*, pp. 1-8, 2020, doi: 10.1109/ICCES51560.2020.9334581.

[13] L. J. Jeremy, C. A. Ooi, and J. Teh, "Non-isolated conventional DC-DC converter comparison for a photovoltaic system: A review," *Journal of Renewable and Sustainable Energy*, vol. 12, no. 1, 2020, doi: 10.1063/1.5095811.

[14] T. W. Hariyadi and A. Adriansyah, "Comparison of DC-DC Converters Boost Type in Optimizing the Use of Solar Panels," *2020 2nd International Conference on Broadband Communications, Wireless Sensors and Powering, BCWSP 2020*, pp. 189–194, 2020, doi: 10.1109/BCWSP50066.2020.9249464.

[15] M. S. Simoiu, V. Calofir, S. S. Iliescu, I. Fagarasan, and N. Arghira, "BOOST converter modelling as a subsystem of a photovoltaic panel control system," *2020 22nd IEEE International Conference on Automation, Quality and Testing, Robotics - THETA, AQTR 2020 - Proceedings*, pp. 1-6, 2020, doi: 10.1109/AQTR49680.2020.9129963.

[16] J. López Seguel, S. I. Seleme, and L. M. F. Morais, "Comparison of the performance of MPPT methods applied in converters buck and buck-boost for autonomous photovoltaic systems," *Ingeniare*, vol. 29, no. 2, pp. 229–244, 2021, doi: 10.4067/S0718-33052021000200229.

[17] I. Achmad and Anggara Trisna Nugraha, "Implementation of Voltage Stabilizers on Solar Cell System Using Buck-Boost Converter," in *Journal of Electronics, Electromedical Engineering, and Medical Informatics*, vol. 4, no. 3, pp. 154–160, 2022, doi: 10.35882/jeeemi.v4i3.246.

[18] A. J. O. Hanfesh, J. Mohammed, I. Salman, H. Mohammed, and M. Ali, "Design and implementation of a solar tracking system using a hydraulic system," *AIP Conference Proceedings*, vol. 3002, no. 1, 2024, doi: 10.1063/5.0205799.

[19] A. Baimyshev, A. Zhakatayev, and H. A. Varol, "Augmenting variable stiffness actuation using reaction wheels," *IEEE Access*, vol. 4, pp. 4618–4628, 2016, doi: 10.1109/ACCESS.2016.2602704.

[20] S. Motahhir, A. El Hammoumi, and A. El Ghzizal, "The most used MPPT algorithms: Review and the suitable low-cost embedded board for each algorithm," *Journal of Cleaner Production*, vol. 246, 2020, doi: 10.1016/j.jclepro.2019.118983.

[21] R. B. Bollipo, S. Mikkili, and P. K. Bonthagorla, "Critical Review on PV MPPT Techniques: Classical, Intelligent and Optimisation," *IET Renewable Power Generation*, vol. 14, no. 9, pp. 1433–1452, 2020, doi: 10.1049/iet-rpg.2019.1163.

[22] M. L. Katche, A. B. Makokha, S. O. Zachary, and M. S. Adaramola, "A Comprehensive Review of Maximum Power Point Tracking (MPPT) Techniques Used in Solar PV Systems," *Energies*, vol. 16, no. 5, 2023, doi: 10.3390/en16052206.

[23] S. Bhattacharyya, D. S. Kumar P, S. Samanta, and S. Mishra, "Steady output and fast tracking MPPT (SOFT-MPPT) for P&O and InC algorithms," *IEEE Transactions on Sustainable Energy*, vol. 12, no. 1, pp. 293–302, 2021, doi: 10.1109/TSTE.2020.2991768.

[24] P. T. Szemes and M. Melhem, "Analyzing and modeling PV with 'P&O' MPPT Algorithm by MATLAB/Simulink," *2020 3rd International Symposium on Small-Scale Intelligent Manufacturing Systems, SIMS 2020*, pp. 1-6, 2020, doi: 10.1109/SIMS49386.2020.9121579.

[25] N. F. Ibrahim *et al.*, "A new adaptive MPPT technique using an improved INC algorithm supported by fuzzy self-tuning controller for a grid-linked photovoltaic system," *PLoS ONE*, vol. 18, no. 11, pp. 1–22, 2023, doi: 10.1371/journal.pone.0293613.

[26] M. Jain, V. Saihjpal, N. Singh, and S. B. Singh, "An Overview of Variants and Advancements of PSO Algorithm," *Applied Sciences (Switzerland)*, vol. 12, no. 17, pp. 1–21, 2022, doi: 10.3390/app12178392.

[27] M. Periasamy, T. Kaliannan, S. Selvaraj, V. Manickam, S. A. Joseph, and J. R. Albert, "Various PSO methods investigation in renewable and nonrenewable sources," *International Journal of Power Electronics and Drive Systems*, vol. 13, no. 4, pp. 2498–2505, 2022, doi: 10.11591/ijpeds.v13.i4.pp2498-2505.

[28] S. R. Revathy *et al.*, "Design and Analysis of ANFIS - Based MPPT Method for Solar Photovoltaic Applications," *International Journal of Photoenergy*, vol. 2022, 2022, doi: 10.1155/2022/9625564.

[29] M. R. Javed, A. Waleed, U. S. Virk, and S. Z. Ul Hassan, "Comparison of the Adaptive Neural-Fuzzy Interface System (ANFIS) based Solar Maximum Power Point Tracking (MPPT) with other Solar MPPT Methods," *Proceedings - 2020 23rd IEEE International Multi-Topic Conference, INMIC 2020*, pp. 1-5, 2020, doi: 10.1109/INMIC50486.2020.9318178.

[30] C. G. Villegas-Mier, J. Rodriguez-Resendiz, J. M. Álvarez-Alvarado, H. Rodriguez-Resendiz, A. M. Herrera-Navarro, and O. Rodríguez-Abreo, "Artificial neural networks in mppt algorithms for optimization of photovoltaic power systems: A review," *Micromachines*, vol. 12, no. 10, pp. 1–19, 2021, doi: 10.3390/mi12101260.

[31] A. Gündoğdu and R. Çelikel, "ANN-Based MPPT Algorithm for Photovoltaic Systems," *Turkish Journal of Science & Technology*, vol. 15, no. 2, pp. 101–110, 2020.

[32] M. N. Ali, K. Mahmoud, M. Lehtonen, and M. M. F. Darwish, "Promising mppt methods combining metaheuristic, fuzzy-logic and ann techniques for grid-connected photovoltaic," *Sensors (Switzerland)*, vol. 21, no. 4, pp. 1–18, 2021, doi: 10.3390/s21041244.

[33] S. A. Sarang *et al.*, "Maximizing solar power generation through conventional and digital MPPT techniques: a comparative analysis," *Scientific Reports*, vol. 14, no. 1, pp. 1–18, 2024, doi: 10.1038/s41598-024-59776-z.

[34] R. J. Yang *et al.*, "Digitalizing building integrated photovoltaic (BIPV) conceptual design: A framework and an example platform," *Building and Environment*, vol. 243, p. 110675, 2023, doi: 10.1016/j.buildenv.2023.110675.

[35] McKinsey, "Quantum Computing: Potential and Challenges ahead," *Plain concepts*, 2024, https://www.plainconcepts.com/quantum-computing-potential-challenges/.

[36] A. A. Jadallah, A. O. Hanfesh, and T. H. Jebur, "Design, fabrication, testing and simulation of a modern glass to glass photovoltaic module in Iraq," *Journal of Engineering Science and Technology*, vol. 13, no. 9, pp. 2750–2764, 2018.

[37] M. Albaker Najm abed, A. Abdul Razzaq Altahir, and A. Abdulhadi ◌Al-Moadhen, "A Review of Hybrid Electric Vehicle Configurations: Advances and Challenges," *Kerbala Journal for Engineering Sciences*, vol. 4, no. 3, pp. 259–282, 2024, doi: 10.63463/kjes1155.

[38] I. Kaaya *et al.*, "A physics-based framework for modelling the performance and reliability of BIPV systems," *Solar Energy*, vol. 277, p. 112730, 2024, doi: 10.1016/j.solener.2024.112730.

[39] D. Sarkar, A. Kumar, and P. K. Sadhu, "A Survey on Development and Recent Trends of Renewable Energy Generation from BIPV Systems," *IETE Technical Review (Institution of Electronics and Telecommunication Engineers, India)*, vol. 37, no. 3, pp. 258–280, 2020, doi: 10.1080/02564602.2019.1598294.

[40] Z. Liu *et al.*, "A comprehensive study of feasibility and applicability of building integrated photovoltaic (BIPV) systems in regions with high solar irradiance," *Journal of Cleaner Production*, vol. 307, p. 127240, 2021, doi: 10.1016/j.jclepro.2021.127240.

[41] K. Ishaque, Z. Salam, and H. Taheri, "Accurate MATLAB simulink PV system simulator based on a two-diode model," *Journal of Power Electronics*, vol. 11, no. 2, pp. 179–187, 2011, doi: 10.6113/JPE.2011.11.2.179.

[42] V. Stornelli, M. Muttillo, T. de Rubeis, and I. Nardi, "A new simplified five-parameter estimation method for single-diode model of photovoltaic panels," *Energies*, vol. 12, no. 22, 2019, doi: 10.3390/en12224271.

[43] M. A. Najm Abed, A. Abdul Razzaq Altahir, A. O. Hanfesh, and A. A. Ahmed, "Performance Evaluation of PMSM and BLDC Motors in Different Operating Scenarios Based Slide Mode Control," *2024 4th International Conference on Electrical Machines and Drives, ICEMD 2024*, pp. 24–25, 2024, doi: 10.1109/ICEMD64575.2024.10963593.

[44] I. A. R. Hameed, A. A. R. Altahir, and H. S. Hameed, "An investigation of solar PV systems coupled with diesel generators: Opportunities and challenges," in *AIP Conference Proceedings*, vol. 2631, 2023, doi: 10.1063/5.0133658.

[45] A. Pradhan and B. Panda, "A simplified design and modeling of boost converter for photovoltaic sytem," *International Journal of Electrical and Computer Engineering*, vol. 8, no. 1, pp. 141–149, 2018, doi: 10.11591/ijece.v8i1.pp141-149.

[46] M. N. Huynh, H. N. Duong, and V. H. Nguyen, "A Passivity-based Control Combined with Sliding Mode Control for a DC-DC Boost Power Converter," *Journal of Robotics and Control (JRC)*, vol. 4, no. 6, pp. 780–790, 2023, doi: 10.18196/jrc.v4i6.20071.

[47] D. Yan *et al*., "Review of general modeling approaches of power converters," in *Chinese Journal of Electrical Engineering*, vol. 7, no. 1, pp. 27-36, March 2021, doi: 10.23919/CJEE.2021.000002.

[48] M. F. Guepfrih, G. Waltrich, and T. B. Lazzarin, "High Step-Up DC-DC Converter Using Built-In Transformer Voltage Multiplier Cell and Dual Boost Concepts," *IEEE Journal of Emerging and Selected Topics in Power Electronics*, vol. 9, no. 6, pp. 6700–6712, 2021, doi: 10.1109/JESTPE.2021.3063060.

[49] M. Meraj, M. S. Bhaskar, A. Iqbal, N. Al-Emadi, and S. Rahman, "Interleaved Multilevel Boost Converter with Minimal Voltage Multiplier Components for High-Voltage Step-Up Applications," *IEEE Transactions on Power Electronics*, vol. 35, no. 12, pp. 12816–12833, 2020, doi: 10.1109/TPEL.2020.2992602.

[50] M. Rezaie and V. Abbasi, "Ultrahigh Step-Up DC-DC Converter Composed of Two Stages Boost Converter, Coupled Inductor, and Multiplier Cell," *IEEE Transactions on Industrial Electronics*, vol. 69, no. 6, pp. 5867–5878, 2022, doi: 10.1109/TIE.2021.3091916.

[51] R. Saravanan and N. Jaya, "Multistage Boost Converter with Modified Voltage Multiplier for Contemporary Applications," *Journal of Electrical Engineering and Technology*, vol. 19, no. 7, pp. 4323–4333, 2024, doi: 10.1007/s42835-024-01857-0.

[52] X. Fan, H. Sun, Z. Yuan, Z. Li, R. Shi, and N. Ghadimi, "High Voltage Gain DC/DC Converter Using Coupled Inductor and VM Techniques," *IEEE Access*, vol. 8, pp. 131975–131987, 2020, doi: 10.1109/ACCESS.2020.3002902.

[53] T. Sutikno, A. S. Samosir, R. A. Aprilianto, H. S. Purnama, W. Arsadiando, and S. Padmanaban, "Advanced DC-DC converter topologies for solar energy harvesting applications: A review," *Clean Energy*, vol. 7, no. 3, pp. 555–570, 2023, doi: 10.1093/ce/zkad003.

[54] S. Shao *et al.*, "Modeling and Advanced Control of Dual-Active-Bridge DC-DC Converters: A Review," *IEEE Transactions on Power Electronics*, vol. 37, no. 2, pp. 1524–1547, 2022, doi: 10.1109/TPEL.2021.3108157.

[55] Q. Xu, N. Vafamand, L. Chen, T. Dragicevic, L. Xie, and F. Blaabjerg, "Review on Advanced Control Technologies for Bidirectional DC/DC Converters in DC Microgrids," *IEEE Journal of Emerging and Selected Topics in Power Electronics*, vol. 9, no. 2, pp. 1205–1221, 2021, doi: 10.1109/JESTPE.2020.2978064.

[56] I. N. Issa, A. A. R. Altahir, and F. M. Tuaimah, "Choosing PSO under Different Overloads to Provide Best Power Flow for IEEE - 57 Bus," *Al-Iraqia Journal for Scientific Engineering Research*, vol. 2, no. 3, pp. 64–73, 2023, doi: 10.58564/ijser.2.3.2023.88.

[57] P. Mohseni, S. Mohammadsalehian, M. R. Islam, K. M. Muttaqi, D. Sutanto, and P. Alavi, "Ultrahigh Voltage Gain DC-DC Boost Converter with ZVS Switching Realization and Coupled Inductor Extendable Voltage Multiplier Cell Techniques," *IEEE Transactions on Industrial Electronics*, vol. 69, no. 1, pp. 323–335, 2022, doi: 10.1109/TIE.2021.3050385.

[58] A. Wong, D. Rexachs, and E. Luque, "Parallel Application Signature for Performance Analysis and Prediction," *IEEE Transactions on Parallel and Distributed Systems*, vol. 26, no. 7, pp. 2009–2019, 2015, doi: 10.1109/TPDS.2014.2329688.

[59] N. J. Hadi and A. A. R. A.- Tahir, "Study Of Thermal Solar Energy Storage Using Stationary Batterirs and Melting Salts Technique," *Repository of Open Acces Papers*, no. 2, 2006.

[60] Q. A. Mahdi *et al.*, "Development of Estimation and Forecasting Method in Intelligent Decision Support Systems," *Eastern-European Journal of Enterprise Technologies*, vol. 3, pp. 51–62, 2021, doi: 10.15587/1729-4061.2021.232718.

[61] B. Zhu, S. Hu, G. Liu, Y. Huang, and X. She, "Low-Voltage Stress Buck-Boost Converter with a High-Voltage Conversion Gain," *IEEE Access*, vol. 8, pp. 95188–95196, 2020, doi: 10.1109/ACCESS.2020.2995889.

[62] A. M. S. S. Andrade, E. Mattos, L. Schuch, H. L. Hey, and M. L. Da Silva Martins, "Synthesis and Comparative Analysis of Very High Step-Up DC-DC Converters Adopting Coupled-Inductor and Voltage Multiplier Cells," *IEEE Transactions on Power Electronics*, vol. 33, no. 7, pp. 5880–5897, 2018, doi: 10.1109/TPEL.2017.2742900.

[63] N. Ncir and N. El Akchioui, "An advanced intelligent MPPT control strategy based on the imperialist competitive algorithm and artificial neural networks," *Evolutionary Intelligence*, vol. 17, no. 3, pp. 1437–1461, 2024, doi: 10.1007/s12065-023-00838-y.

[64] R. B. Bollipo, S. Mikkili, and P. K. Bonthagorla, "Critical Review on PV MPPT Techniques: Classical, Intelligent and Optimisation," *IET Renewable Power Generation*, vol. 14, no. 9, pp. 1433–1452, 2020, doi: 10.1049/iet-rpg.2019.1163.

[65] M. Fathi and J. A. Parian, "Intelligent MPPT for photovoltaic panels using a novel fuzzy logic and artificial neural networks based on evolutionary algorithms," *Energy Reports*, vol. 7, pp. 1338–1348, 2021, doi: 10.1016/j.egyr.2021.02.051.

[66] R. B. Bollipo, S. Mikkili, and P. K. Bonthagorla, "Hybrid, optimal, intelligent and classical PV MPPT techniques: A review," *CSEE Journal of Power and Energy Systems*, vol. 7, no. 1, pp. 9–33, 2021, doi: 10.17775/CSEEJPES.2019.02720.

[67] K. Y. Yap, C. R. Sarimuthu, and J. M. Y. Lim, "Artificial Intelligence Based MPPT Techniques for Solar Power System: A review," *Journal of Modern Power Systems and Clean Energy*, vol. 8, no. 6, pp. 1043–1059, 2020, doi: 10.35833/MPCE.2020.000159.

[68] N. S. Abu, W. M. Bukhari, M. H. Adli, H. Maghfiroh, and A. Ma'arif, "Advancements, Challenges and Safety Implications of AI in Autonomous Vehicles: A Comparative Analysis of Urban vs. Highway Environments," *Journal of Robotics and Control (JRC)*, vol. 5, no. 3, pp. 613–635, 2024, doi: 10.18196/jrc.v5i3.21114.

[69] A. S. T. Hussain *et al.*, "Unlocking Solar Potential: Advancements in Automated Solar Tracking Systems for Enhanced Energy Utilization," *Journal of Robotics and Control (JRC)*, vol. 5, no. 4, pp. 1018–1027, 2024, doi: 10.18196/jrc.v5i4.19931.

[70] A. Saleh, K. S. F. Azmi, T. Hardianto, and W. Hadi, "Comparison of MPPT fuzzy logic controller based on perturb and observe (P&O) and incremental conductance (InC) algorithm on buck-boost converter," in *Proceedings - 2018 2nd International Conference on Electrical Engineering and Informatics: Toward the Most Efficient Way of Making and Dealing with Future Electrical Power System and Big Data Analysis, ICon EEI 2018*, pp. 154–158, 2018, doi: 10.1109/ICon-EEI.2018.8784324.

[71] O. N. Rajab Al-Jaboury, Z. Hamodat, and R. W. Daoud, "Design of Power Control Circuit for Grid-Connected PV System-Based Neural Network," *Journal of Robotics and Control (JRC)*, vol. 5, no. 3, pp. 821–828, 2024, doi: 10.18196/jrc.v5i3.20751.

[72] A. P. Yoganandini and G. S. Anitha, "A modified particle swarm optimization algorithm to enhance MPPT in the PV array," *International Journal of Electrical and Computer Engineering*, vol. 10, no. 5, pp. 5001–5008, 2020, doi: 10.11591/IJECE.V10I5.PP5001-5008.

[73] Q. A. Mahdi *et al*., "Development of a Method for Training Artificial Neural Networks for Intelligent Decision Support Systems," *Eastern-European Journal of Enterprise Technologies*, vol. 1, no. 9–115, pp. 35–44, 2022, doi: 10.15587/1729-4061.2022.251637.

[74] S. Abboud *et al*., "Optimizing Solar Energy Production in Partially Shaded PV Systems with PSO-INC Hybrid Control," *Journal of Robotics and Control (JRC)*, vol. 5, no. 2, pp. 312–320, 2024, doi: 10.18196/jrc.v5i2.20896.

[75] A. A. Mutlag, M. K. Abd, and S. W. Shneen, "Power Management and Voltage Regulation in DC Microgrid with Solar Panels and Battery Storage System," *Journal of Robotics and Control (JRC)*, vol. 5, no. 2, pp. 397–407, 2024, doi: 10.18196/jrc.v5i2.20581.

[76] S. W. Shneen, M. K. Abd, and A. A. Mutlag, "Voltage Regulation and Power Management of DC Microgrid with Photovoltaic/Battery Storage System Using Flatness Control Method," *Journal of Robotics and Control (JRC)*, vol. 5, no. 6, pp. 1664–1672, 2024, doi: 10.18196/jrc.v5i6.22530.

[77] M. Q. Yu, "Parameter Identification of Photovoltaic Cell Model Based on Perturbation and Observation and Modified Gauss-Newton Method," in *Chinese Control Conference, CCC*, pp. 6127–6131, 2018, doi: 10.23919/ChiCC.2018.8483101.

[78] K. Amara *et al.*, "Improved Performance of a PV Solar Panel with Adaptive Neuro Fuzzy Inference System ANFIS based MPPT," in *7th International IEEE Conference on Renewable Energy Research and Applications, ICRERA 2018*, pp. 1098–1101, 2018, doi: 10.1109/ICRERA.2018.8566818.

[79] A. S. Mahdi, A. K. Mahamad, S. Saon, T. Tuwoso, H. Elmunsyah, and S. W. Mudjanarko, "Maximum power point tracking using perturb and observe, fuzzy logic and ANFIS," *SN Applied Sciences*, vol. 2, no. 1, p. 89, 2020, doi: 10.1007/s42452-019-1886-1.

[80] K. H. Tajaldin and H. J. Motlak, "Enhancement of DC-DC Luo Converter Using Adaptive PI MPPT and P&O MPPT for Photovoltaic System," *Journal Europeen des Systemes Automatises*, vol. 57, no. 3, pp. 921–933, 2024, doi: 10.18280/jesa.570330.